

1 **Supplementary Method 1: Calculation of other parameters from meta-analysis**

2 Sulfur oxidation ratio (SOR) and nitrogen oxidation ratio (NOR) are indicators of
3 secondary pollutant transformation in the atmosphere (Sun et al., 2006; Xu et al., 2017).

4 Higher SOR and NOR values imply greater oxidation of gaseous species to sulfate- and
5 nitrate-containing secondary particles (Sun et al., 2006), respectively. Their formulae
6 are as follows, where n refers to the molar concentrations:

7 $SOR = nSO_4^{2-} / (nSO_4^{2-} + nSO_2)$ (1)

8 $NOR = nNO_3^- / (nNO_3^- + nNO_2)$ (2)

9 To identify whether acidic species are fully neutralized by NH₃ in PM_{2.5}, we selected
10 two indicators: the slope of the linear regression between equivalent concentrations of
11 [NH₄⁺] and [SO₄²⁻] and the slope of the linear regression between equivalent
12 concentrations of [NH₄⁺] and [SO₄²⁻ + NO₃⁻] (Sun et al., 2006). In the atmosphere, NH₃
13 is first taken up by sulfuric acid to form ammonium sulfate salts and then any excess
14 NH₃ may then react with nitric and hydrochloric acids to form ammonium nitrate and
15 ammonium chloride (Ianniello et al., 2010). When the slope of NS is less than 1, NH₃
16 is not completely neutralized with sulfuric acid and nitric acid, suggesting a NH₃-
17 limited environment. Slopes of NS and NSN greater than 1 indicate that they reacted
18 completely, suggesting a NH₃-rich environment (Xu et al., 2017).

19 **Supplementary Method 2: Additional information about the monitoring data**

20 The concentrations of PM_{2.5}, SO₂, and NO₂ were measured at state-controlled air
21 sampling sites located within each city or county. To avoid direct influence of potential
22 air pollution sources, most of the monitoring sites were situated in background locations
23 in the urban areas. Concentrations of PM_{2.5} were measured using the micro oscillating

balance method (TEOM from Rupprecht & Patashnick Co., Inc., USA) or the β absorption method (BAM 1020 from Met One Instrument Inc., USA; Tianhong Co., China or Xianhe Co., China). Concentrations of SO_2 were measured using either UV-spectrophotometry (TEI Model 49i from Thermo Fisher Scientific Inc., USA) or Ultraviolet Fluorescence (TEI Model 43i from Thermo Fisher Scientific Inc., USA) methods, and concentrations of NO_2 using the chemiluminescence (TEI Model 42i from Thermo Fisher Scientific Inc., USA) method. The detection limits (DL) of these techniques are sufficient to measure accurately the high or relatively high concentration of $\text{PM}_{2.5}$, SO_2 , and NO_2 at all monitoring sites.

Data from all monitoring sites were automatically released to an open website after validation using HJ630-2011 specifications (<http://kjs.mep.gov.cn/hjbhbz/bzwb/other/qt/201109/W020120130585014685198.pdf>). The instruments for $\text{PM}_{2.5}$ measurements were tested using the reference method by at least three samples based on HJ 618 specifications. The instruments used for SO_2 and NO_2 measurement at each site were tested for zero and scale noises, error of indication, zero and span drifts, etc.

Along with the acid gases, surface NH_3 concentrations over China for the 2008–2016 period (the current availability) was extracted from the study of Liu et al. (2019), which were estimated using IASI (the Infrared Atmospheric Sounding Interferometer) NH_3 retrievals and NH_3 vertical profiles (Fig S5). Although the satellite-derived surface NH_3 concentrations are described in detail by Liu et al. (2019), a brief summary is given here for the reader's convenience. The NH_3 total columns were derived from the IASI-A instrument (aboard the MetOp-A platform) morning overpass observations (i.e.,

47 09:30 local time at the Equator during overpass), which have a circular footprint of 12
48 km diameter at nadir and an ellipsoid shaped footprint of up to 20 km × 39 km at the
49 maximum diameter ([Van Damme et al., 2018](#)). The IASI NH₃ datasets are the ANNI-
50 NH₃-v2.2R-I retrieval product, which was developed by converting hyperspectral range
51 index data to NH₃ columns using an Artificial Neural Network for IASI (ANNI)
52 algorithm ([Whitburn et al., 2016](#)). The NH₃ vertical profiles were simulated from the
53 Goddard Earth Observing System-Chemistry (GEOS-Chem) atmospheric transport
54 model considering H₂SO₄-HNO₃-NH₃ aerosol thermodynamics mechanisms ([Whitburn](#)
55 [et al., 2016; Van Damme et al., 2017](#)), and were used to convert the satellite NH₃
56 columns to surface NH₃ concentrations. The satellite NH₃ predictions are reliable
57 (average R² = 0.919 and p<0.001) by validating against the in-situ surface observations
58 on a monthly basis ([Liu et al., 2019](#))

59 **Supplementary Method 3: WRF-CMAQ model evaluation**

60 The monthly predicted PM_{2.5} concentrations were compared with the observations
61 retrieved by the Space-Time Extra-Tree (STET) model ([Wei et al., 2020,2021](#)). The
62 STET model provided a high resolution (1 km) of PM_{2.5} concentration dataset supported
63 by the Moderate Resolution Imaging Spectroradiometer (MODIS) satellite
64 observations and thus can be used to evaluate the model performances. Supplementary
65 Fig. S3 shows that the model underestimated the PM_{2.5} concentration in Xinjiang
66 province, which was caused by missing sources in the emission inventory in Xinjiang
67 province. Overall, as shown in Supplementary Fig. S3, the WRF-CMAQ model
68 captured similar spatial distributions to the STET model, with high levels of PM_{2.5}
69 concentrations occurring in the central parts of China including the Beijing-Tianjin-
70 Hebei region and the Sichuan basin.

71 The simulations of temperature at 2 m above the ground (T2), wind speed (WS), and
72 relative humidity (RH) versus observed values at 400 monitoring sites in China are
73 shown in Supplementary Fig. S4. The meteorological measurements used for the model
74 performances were obtained from the National Climate Data Center (NCDC)
75 (<ftp://ftp.ncdc.noaa.gov/pub/data/noaa/>). The comparisons showed that the model
76 performed well at predicting meteorological parameters with R values of 0.94, 0.64 and
77 0.82 for T2, WS and RH, respectively. The WS were overestimated in most regions of
78 China, as widely reported in previous studies (Gao et al., 2016; Chen et al., 2019),
79 which may relate to the underlying surface parameters set in the WRF model
80 configurations.

81

82

83

84

85

86

87

88

89

90

91

92

93

94 **Figure captions**

95 **Figure S1.** Spatial distribution of the 1498 monitoring sites (blue dots) and the 218
96 meta-analysis sites (red dots).

97 **Figure S2.** Timeline of policies to improve air quality in China. The green text indicates
98 the start of control policies from the Chinese government for the pollutant highlighted;
99 the * symbol and red text indicates the pollutant emission reduction target in the given
100 5-year plan. The different background colors denote the three different pollutant history
101 periods (Periods I, II and III) described in the main text.

102 **Figure S3.** Simulated (a) and observed (b) monthly mean PM_{2.5} concentrations ($\mu\text{g m}^{-3}$)
103 for January 2010. The observations are from the Space-Time Extra-Tree (STET)
104 model which provides a high spatial resolution (1 km) PM_{2.5} concentration dataset.

105 **Figure S4.** The left column shows simulated (shaded) and observed (dot) monthly-
106 mean temperature at 2 m above the ground (T2) (a), wind speed (WS) (b), and (c)
107 relative humidity (RH) for January 2010. The right column shows scatterplots of
108 simulated versus observed T2, WS, RH at 400 monitoring sites in China. The value of
109 correlation coefficients (R) is presented on each scatterplot.

110 **Figure S5.** (a) Spatial patterns of trends between 2008 and 2016 in annual mean
111 concentrations of NH₃. (b) Annual average ground-based measured NH₃ concentrations
112 2008-2016 across all of China and in northern and southern regions. Data for map (a)
113 are from NH₃ satellite retrievals combining vertical profiles from Goddard Earth
114 Observing System-Chemistry (GEOS-Chem).

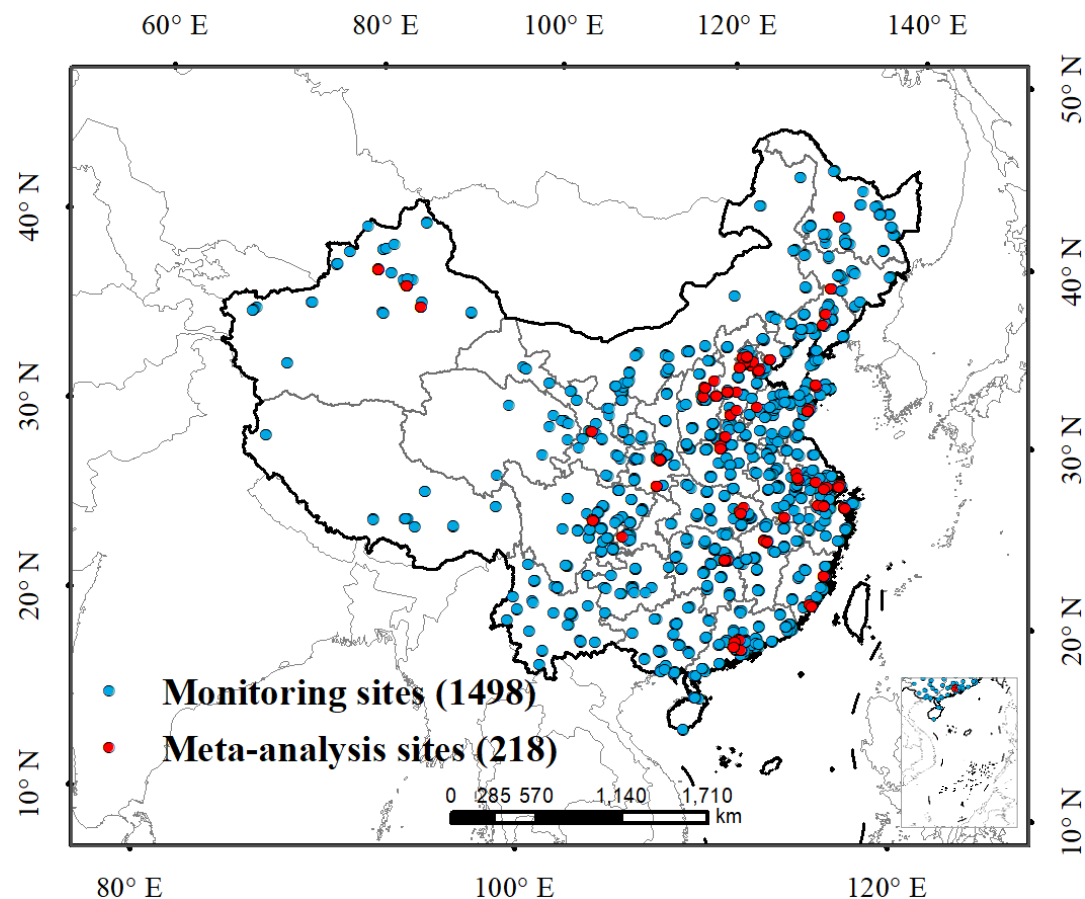
115 **Figure S6.** Simulated PM_{2.5} concentrations (in $\mu\text{g m}^{-3}$) without (basic) and with 50%
116 ammonia (NH₃) emissions reductions in January for the years 2010, 2014, 2017 and
117 2020 in four megacity clusters (BTH: Beijing-Tianjin-Hebei, YRD: Yangtze River
118 Delta, SCB: Sichuan Basin, PRD: Pearl River Delta). Inset maps indicate the location
119 of each region. ** denotes significant difference without and with 50% ammonia
120 emission reductions ($P < 0.05$). n is the number of calculated samples by grid extraction.
121 Error bars are standard errors of means. (Period I (2000–2012), Period II (2013–2016),
122 and Period III (2017–2019); Special control is the restrictions in economic activities
123 and associated emissions during the COVID-19 lockdown period in 2020).

124 **Figure S7.** The spatial distributions of simulated SIA concentrations (in $\mu\text{g m}^{-3}$)
125 without (a) and with (b) 50% ammonia emissions reduction for the years 2010, 2014,
126 2017 and 2020. The % decreases in SIA concentrations in each year for the simulations
127 with the emissions reductions are shown in row (c). (Period I (2000–2012), Period II
128 (2013–2016), and Period III (2017–2019); Special control is the restrictions in
129 economic activities and associated emissions during the COVID-19 lockdown period
130 in 2020).

131 **Figure S8.** The spatial distributions of simulated PM_{2.5} concentrations (in $\mu\text{g m}^{-3}$)
132 without (a) and with (b) 50% ammonia emissions reduction for the years 2010, 2014,
133 2017 and 2020. The % decreases in PM_{2.5} concentrations in each year for the
134 simulations with the emissions reductions are shown in row (c). (Period I (2000–2012),
135 Period II (2013–2016), and Period III (2017–2019); Special control is the restrictions
136 in economic activities and associated emissions during the COVID-19 lockdown period
137 in 2020).

138

139 **Figure S1**



140

141

142

143

144

145

146

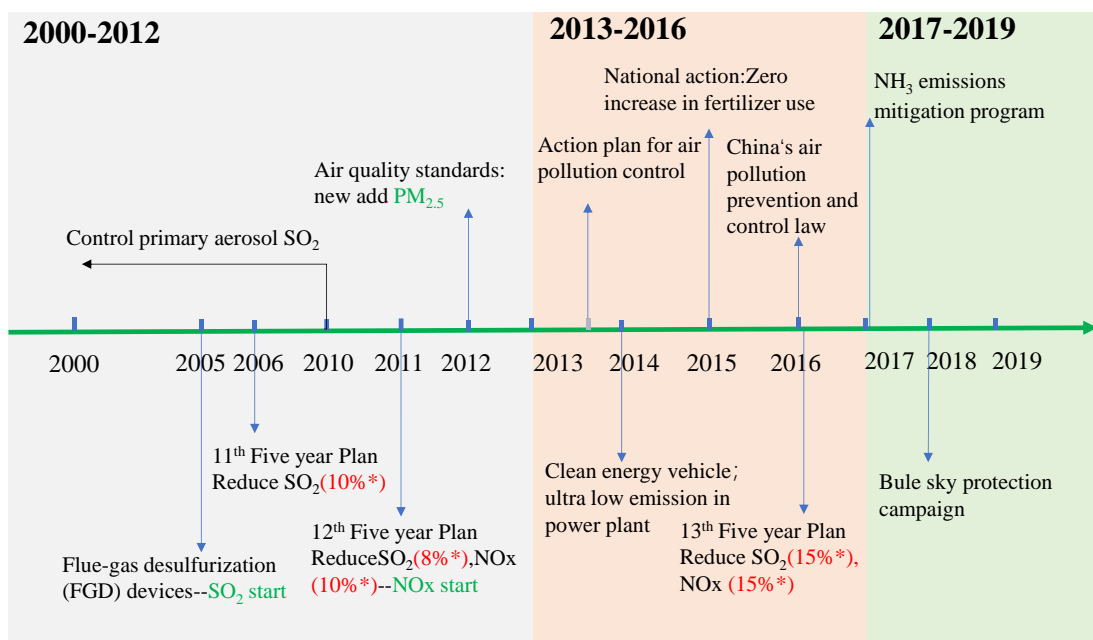
147

148

149

150

151 **Figure S2**



152

153

154

155

156

157

158

159

160

161

162

163

164

165

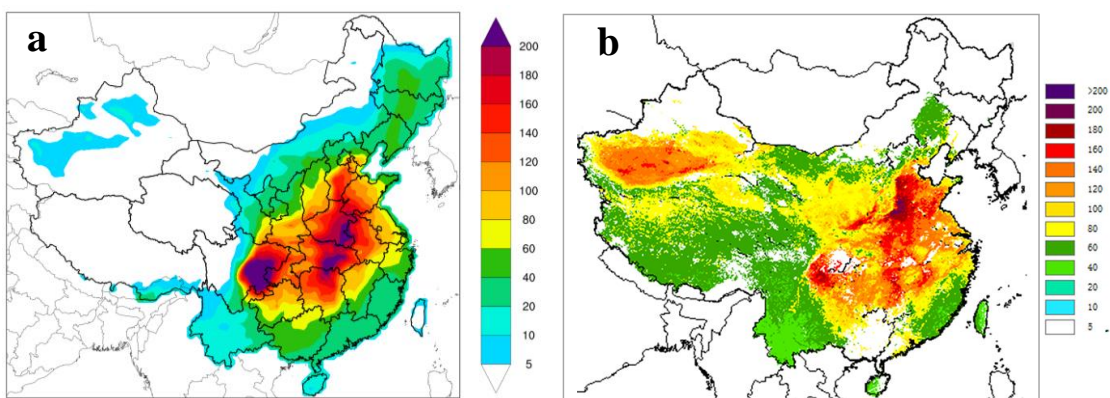
166

167

168

169

170 **Figure S3**



171

172

173

174

175

176

177

178

179

180

181

182

183

184

185

186

187

188

189

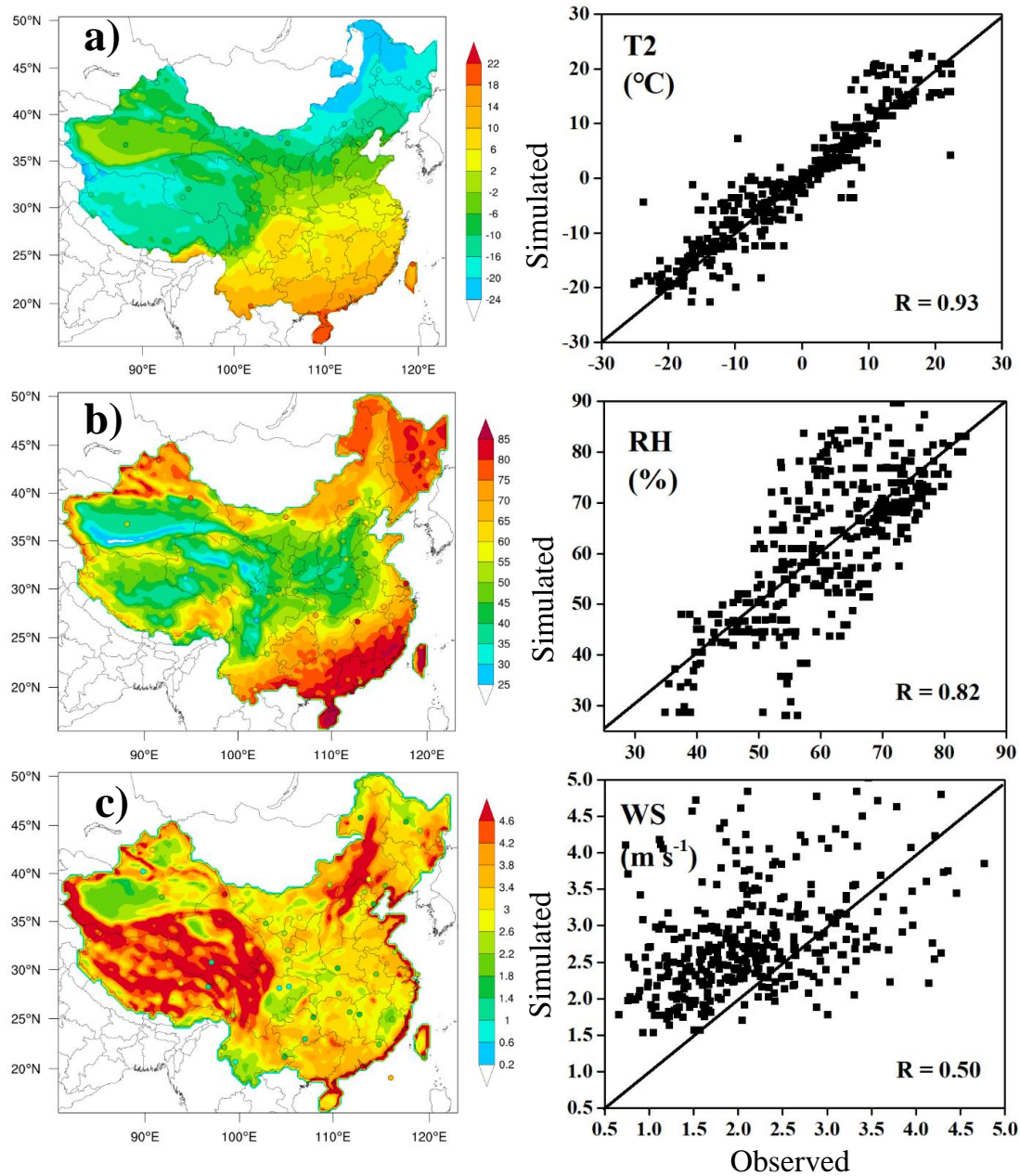
190

191

192

193

194 **Figure S4**



195

196

197

198

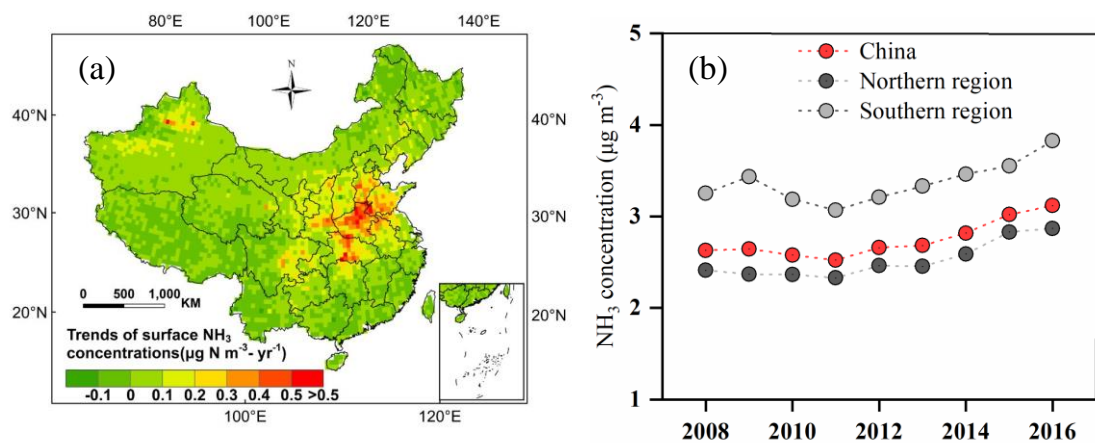
199

200

201

202

203 **Figure S5**



204

205

206

207

208

209

210

211

212

213

214

215

216

217

218

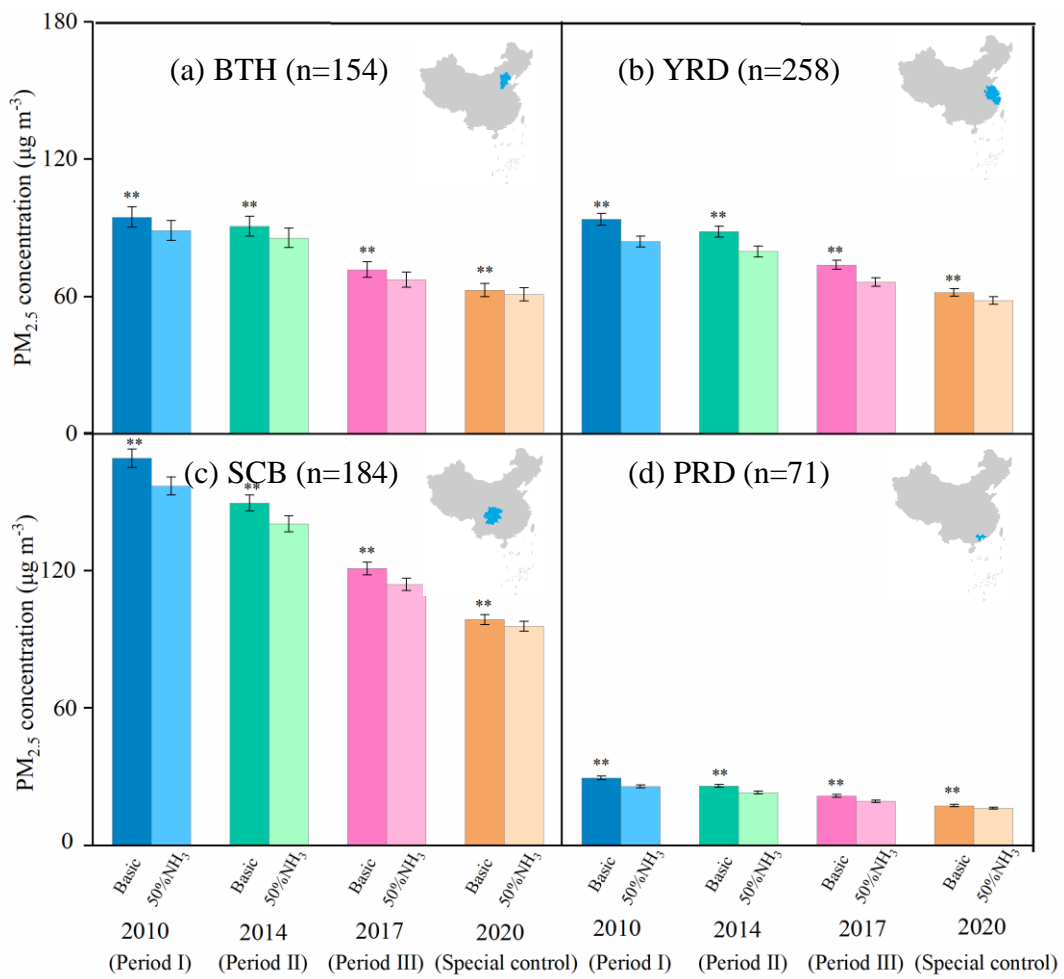
219

220

221

222

223 **Figure S6**



224

225

226

227

228

229

230

231

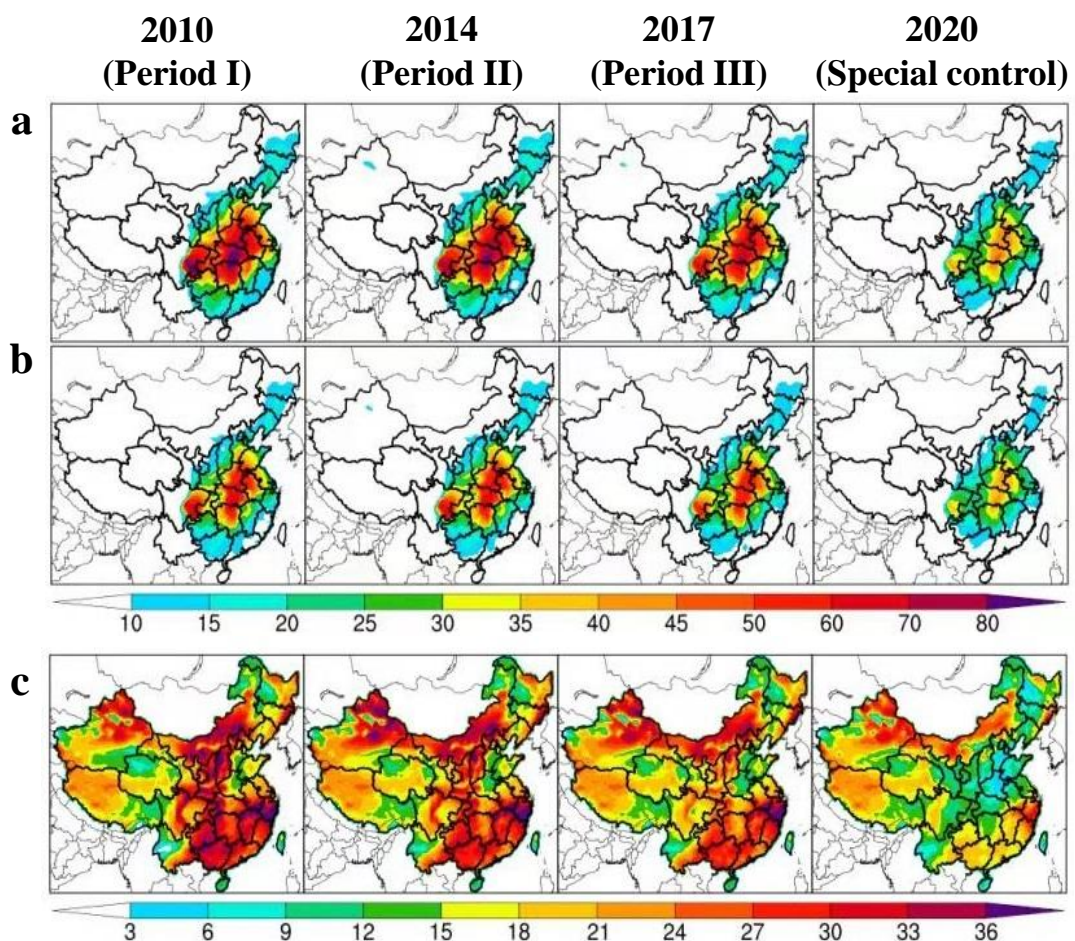
232

233

234

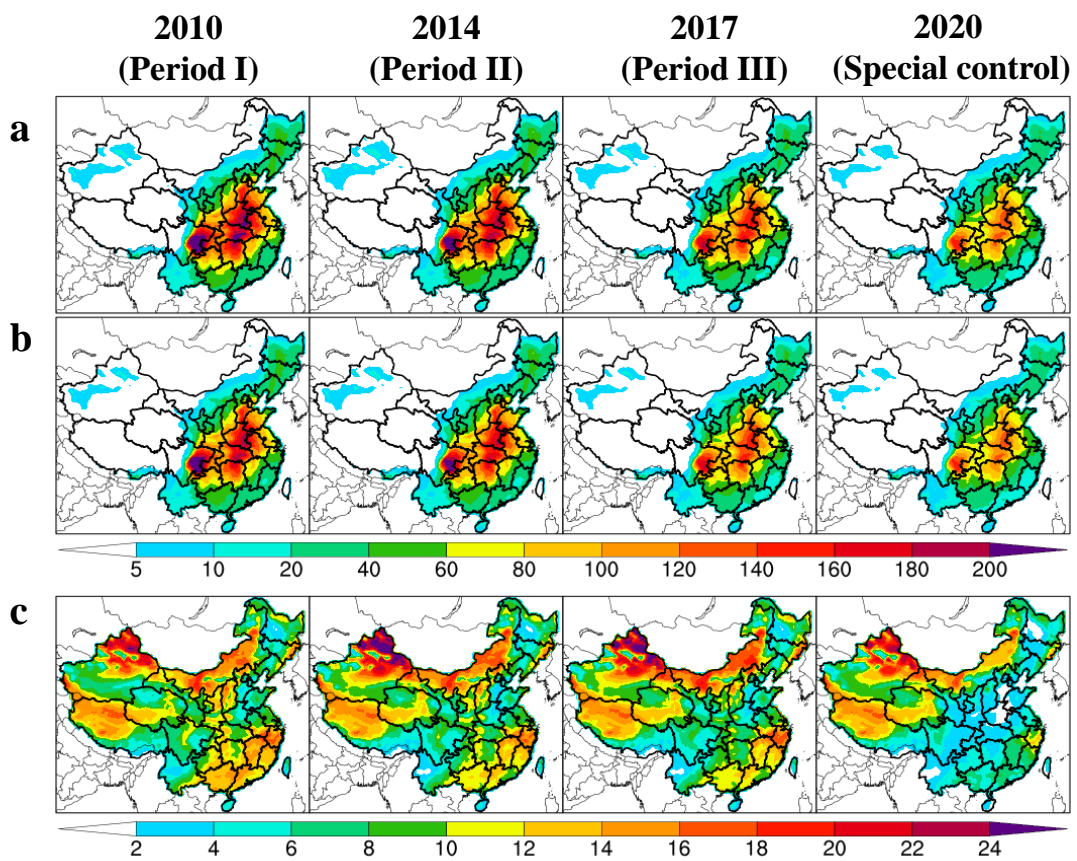
235

236 **Figure S7**



248

249 **Figure S8**



250

251

252

253

254

255

256

257

258

259

260

261

262

263 **Table S1.** Summary of number of measurement sites from different databases assembled
 264 from peer-reviewed publications and used for analyses in the present study of PM_{2.5}
 265 component concentrations, NS, NSN, SOR, and NOR. The details of information in
 266 Supporting Material Dataset. NS is the slope of the regression equation between [NH₄⁺]
 267 and [SO₄²⁻], NSN is the slope of the regression equation between [NH₄⁺] and [SO₄²⁻ +
 268 NO₃⁻], SOR is sulfur oxidation ratio, and NOR is nitrogen oxidation ratio.
 269

	No. of measurement sites	N_{fs} ^a	$5n + 10^b$
OC	84	531290	430
EC	101	396171	515
SO ₄ ²⁻	151	2385388	765
NO ₃ ⁻	175	4542962	885
Cl ⁻	105	886197	535
F ⁻	26	1587	140
NH ₄ ⁺	166	4026300	840
Na ⁺	82	343318	420
K ⁺	91	523882	465
Ca ²⁺	75	88883	385
Mg ²⁺	68	—	350
NS	145	—	735
NSN	144	—	730
SOR	38	—	200
NOR	33	—	175

270 Note: ^a N_{fs} is Rosenberg's fail safe-numbers, calculated to assess the robustness of
 271 findings on PM_{2.5}. ^b n is the number of sites.

272

273

274

275

276 **Table S2.** Anthropogenic emissions of SO₂ in January of 2010, 2014, 2017 and 2020,277 and the percentage decreases in SO₂ emissions between successive pairs of years.

	2010 Tonne	2014 Tonne	2017 Tonne	2020 Tonne	2014-2010 %	2017-2014 %	2020-2017 %
Beijing	20410	10899	4051	2998	-47	-63	-26
Tianjin	29000	22111	9042	7233	-24	-59	-20
Hebei	183194	146125	70877	59536	-20	-51	-16
Shanxi	193721	151346	111566	89253	-22	-26	-20
Inner Mongolia	158304	121932	66986	56938	-23	-45	-15
Liaoning	97766	77459	41043	29551	-21	-47	-28
Jilin	44399	34995	23713	18259	-21	-32	-23
Heilongjiang	44491	43441	28536	20832	-2	-34	-27
Shanghai	43016	28112	14390	8346	-35	-49	-42
Jiangsu	113216	69162	27388	20267	-39	-60	-26
Zhejiang	52789	35704	17846	12671	-32	-50	-29
Anhui	43583	30433	15703	12248	-30	-48	-22
Fujian	37907	19804	13537	9476	-48	-32	-30
Jiangxi	40179	28746	14362	11346	-28	-50	-21
Shandong	244765	178189	84499	63374	-27	-53	-25
Henan	125492	72270	34617	27002	-42	-52	-22
Hubei	182208	112715	69204	53287	-38	-39	-23
Hunan	92142	90407	68003	51002	-2	-25	-25
Guangdong	75644	46140	35595	23849	-39	-23	-33
Guangxi	68551	43141	22565	16247	-37	-48	-28
Hainan	4008	4790	3933	2950	20	-18	-25
Chongqing	120968	67877	35101	23868	-44	-48	-32
Sichuan	113414	75375	37241	27186	-34	-51	-27
Guizhou	191009	181314	111426	83569	-5	-39	-25
Yunnan	66724	54142	33106	24830	-19	-39	-25
Tibet	60	66	97	82	10	47	-15
Shaanxi	105817	76442	40069	32856	-28	-48	-18
Gansu	38708	23976	19749	16590	-38	-18	-16
Qinghai	4778	5594	4310	3362	17	-23	-22
Ningxia	28415	24767	20062	15247	-13	-19	-24
Xinjiang	44162	45561	24929	21190	3	-45	-15
China	2608842	1923034	1103546	845445	-26	-43	-23

278 Note: SO₂ emissions were provided by the Multi-resolution Emission Inventory (MEIC)279 (<http://meicmodel.org>) for the years 2010, 2014 and 2017. The SO₂ emissions of 2020

280 are based on 2017 MEIC as a case of special control following Huang et al. (2021)
281 approach.

282

283

284

285

286

287

288

289

290

291

292

293

294

295

296

297

298

299

300

301

302 **Table S3.** Anthropogenic emissions of NO_x in January of 2010, 2014, 2017 and 2020,
 303 and the percentage decreases in NOx emissions between successive pairs of years.

	2010 Tonne	2014 Tonne	2017 Tonne	2020 Tonne	2014-2010 %	2017-2014 %	2020-2017 %
Beijing	32325	27223	24931	13712	-16	-8	-45
Tianjin	33978	37380	30435	18870	10	-19	-38
Hebei	177625	167812	148367	81602	-6	-12	-45
Shanxi	106872	95243	82741	49645	-11	-13	-40
Inner Mongolia	129645	120068	111328	79043	-7	-7	-29
Liaoning	113719	112970	104711	62826	-1	-7	-40
Jilin	61173	58140	60342	36808	-5	4	-39
Heilongjiang	77226	81565	74725	47077	6	-8	-37
Shanghai	45395	32961	31539	16400	-27	-4	-48
Jiangsu	153102	142730	131740	65870	-7	-8	-50
Zhejiang	95531	75644	71440	35720	-21	-6	-50
Anhui	86796	87662	78304	34454	1	-11	-56
Fujian	47505	41396	46573	22821	-13	13	-51
Jiangxi	39804	39120	34918	16411	-2	-11	-53
Shandong	222442	201757	177591	88796	-9	-12	-50
Henan	137270	126230	105735	45466	-8	-16	-57
Hubei	76893	69558	59338	26702	-10	-15	-55
Hunan	67695	61721	56416	27644	-9	-9	-51
Guangdong	109844	87421	86116	43058	-20	-1	-50
Guangxi	47006	42915	35959	17980	-9	-16	-50
Hainan	6813	7437	7689	4306	9	3	-44
Chongqing	37763	36995	32855	15442	-2	-11	-53
Sichuan	82543	80131	69170	34585	-3	-14	-50
Guizhou	50554	43218	33805	20621	-15	-22	-39
Yunnan	52995	42479	36285	17779	-20	-15	-51
Tibet	2428	2337	3625	2357	-4	55	-35
Shaanxi	58296	56807	48598	26729	-3	-14	-45
Gansu	37634	31398	28059	14871	-17	-11	-47
Qinghai	7872	10535	8907	4810	34	-15	-46
Ningxia	23645	27323	27936	17879	16	2	-36
Xinjiang	42625	62771	48156	31301	47	-23	-35
China	2265015	2110946	1898332	1021583	-7	-10	-46

304 Note: NO_x emissions were provided by the Multi-resolution Emission Inventory (MEIC)
 305 (<http://meicmodel.org>) for the years 2010, 2014 and 2017. The NO_x emissions of 2020

306 are based on 2017 MEIC as a case of special control following Huang et al. (2021)
307 approach.

308

309

310

311

312

313

314

315

316

317

318

319

320

321

322

323

324

325

326

327

328 **Table S4.** Control options for NH₃ emissions reductions with their corresponding
329 estimated percentage emissions reductions (reduction efficiency).

Abatement option	Application processes	Reduction efficiency
Avoiding over-fertilization	Synthetic fertilizer application	>20%
Deep application of fertilizers	Synthetic fertilizer application	~50%
Low crude protein feed	Whole manure management chain	10-40%
Using deep litter in floor and regular washing	Manure in house	20-50%
Covering solid and slurry manure	Manure storage	>60%
Incorporation or plough after spreading	Field application of manure	40-80%
All	NH₃ emissions for all China	30-50%

330 Note: The NH₃ emissions control options and corresponding emissions reduction
331 efficiency are from Liu et al. (2019). The feasible control options can reduce China's
332 NH₃ emissions by 30-50% based on the PKU-NH₃ emission model.
333
334
335
336
337
338
339
340
341
342
343
344

345 **Table S5.** The effectiveness of potential end-of pipe controls on SO₂ and NO_x emissions
346 reductions for different production sectors (unit: %).

Sector	SO ₂	NO _x
Electric	30	31
Industry - building materials	45	59
Industry - boiler	24	7
Industry - steel	—	3
Building	2	—

347 Note: The effectiveness of potential end-of pipe controls on SO₂ and NO_x emissions
348 reductions for different production sectors from Xing et al. (2021). GetData Graph
349 Digitizer (Version 2.25, <http://www.getdatagraph-digitizer.com>) was used to digitize
350 the % effectiveness of SO₂ and NO_x from figures.

351

352

353

354

355

356

357

358

359

360

361 **References**

- 362 Chen, Z. Y., Chen, D. L., Wen, W., Zhuang, Y., Kwan, M. P., Chen, B., Zhao, B., Yang,
363 L., Gao, B. B., Li, R. Y., and Xu, B.: Evaluating the “2+26” regional strategy for air
364 quality improvement during two air pollution alerts in Beijing: Variations in PM_{2.5}
365 concentrations, source apportionment, and the relative contribution of local
366 emission and regional transport, *Atmos. Chem. Phys.*, 19, 6879-6891,
367 <https://doi.org/10.5194/acp-19-6879-2019>, 2019.
- 368 Gao, M., Carmichael, G.R., Wang, Y., Saide, P.E., Yu, M ., Xin, J., Liu, Z., and Wang,
369 Z.: Modeling study of the 2010 regional haze event in the North China Plain, *Atmos.*
370 *Chem. Phys.*, 16, 1673–1691, <https://doi.org/10.5194/acp-16-1673-2016>, 2016.
- 371 Huang, X., Ding, A.J, Gao, J., Zheng, B., Zhou, D.R., Qi, X. M., Tang, R., Wang, J. P.,
372 Ren, C. H., Nie, W., Chi, X. G., Xu, Z., Chen, L. D., Li, Y. Y., Che, F., Pang, N. N.,
373 Wang, H. K., Tong, D., Qin, W., Cheng, W., Liu, W. J., Fu, Q. Y., Liu, B. X., Chai,
374 F. H., Davis, S. J., Zhang, Q., and He, K. B.: Enhanced secondary pollution offset
375 reduction of primary emissions during COVID-19 lockdown in China, *Natl. Sci.*
376 *Rev.*, 8, 137, <https://doi.org/10.1093/nsr/nwaa137>, 2021.
- 377 Ianniello, A., Spataro, F., Esposito, G., Allegrini, I ., Rantica, E ., Ancora,
378 MP., Hu, M., and Zhu, T.: 2010. Occurrence of gas phase ammonia in the area of
379 Beijing (China), *Atmos. Chem. Phys.*, 10, 9487-9503,
380 <https://doi.org/10.5194/acp-10-9487-2010>, 2010.
- 381 Liu, M. X., Huang, X., Song, Y., Tang, J., Cao, J. J ., Zhang, X. Y., Zhang, Q., Wang, S.
382 X., Xu, T. T., Kang, L., Cai, X. H., Zhang, H. S., Yang, F. M., Wang, H. B., Yu, J.
383 Z., Lau, A. K. H., He, L. Y., Huang, X. F., Duan, L., Ding, A. J., Xue, L. K., Gao,
384 J., Liu, B., and Zhu, T.: Ammonia emission control in China would mitigate haze
385 pollution and nitrogen deposition, but worsen acid rain, *Proc. Natl. Acad. Sci. U. S.*

- 386 A., 116, 7760-7765, <https://doi.org/10.1073/pnas.1814880116>, 2019.
- 387 Sun, Y. L., Zhuang, G. S., Tang, A. H., Wang, Y., and An, Z. S.: Chemical characteristics
388 of PM_{2.5} and PM₁₀ in haze-fog episodes in Beijing, Environ. Sci. Technol., 40, 3148-
389 3155, <https://doi.org/10.1021/es051533g>, 2006.
- 390 Van Damme, M. Clarisse, L., Whitburn, S., Hadji-Lazaro, J., Hurtmans, D.,
391 Clerbaux, C., and Coheur, P. F.: Industrial and agricultural ammonia point sources
392 exposed, Nature, 564, 99, <https://doi.org/10.1038/s41586-018-0747-1>, 2018.
- 393 Van Damme, M., Van Damme, M., Clarisse, L., Bauduin, S., Heald, CL., Hadji-
394 Lazaro, J., Hurtmans, D., Zondlo, M.A., Clerbaux, C., and Coheur, P. F.: Version
395 2 of the IASI NH₃ neural network retrieval algorithm: near-real-time and reanalysed
396 datasets, Atmos. Meas. Tech., 10, 4905-4914, <https://doi.org/10.5194/amt-10-4905-2017>, 2017.
- 398 Whitburn, S. Van, Damme, M., Clarisse, L., Bauduin, S., Heald, C. L., Hadji-Lazaro,
399 J., Hurtmans, D., Zondlo, M. A., Clerbaux, C., and Coheur, P. F.: A flexible and
400 robust neural network IASI-NH₃ retrieval algorithm. J. Geophys. Res.-Atmos., 121,
401 6581-6599, <https://doi.org/10.1002/2016JD024828>, 2016.
- 402 Wei, J., Li, Z. Q., Cribb, M., Huang, W., Xue, W.H., Sun, L., Guo, J. P., Peng, Y. R., Li,
403 J., and Lyapustin, A.: Improved 1 km resolution PM_{2.5} estimates across China using
404 enhanced space–time extremely randomized trees, Atmos. Chem. Phys., 20, 3273-
405 3289, <https://doi.org/10.5194/acp-20-3273-2020>, 2020.
- 406 Wei, J., Li, Z. Q., Lyapustin, A., Sun, L., Peng, Y. R., Xue, W. H., Su, T. N., and Cribb,
407 M.: Reconstructing 1-km-resolution high-quality PM_{2.5} data records from 2000 to
408 2018 in China: spatiotemporal variations and policy implications. Remote. Sens.
409 Environ., 252, 112136, <https://doi.org/10.1016/j.rse.2020.112136>, 2021.
- 410 Xing, J., Liu, X., Wang, S. X., Wang, T., Ding, D., Yu, S., Shindell, D., Ou, Y.,

411 Morawska, L., Li, S. W., Ren, L., Zhang, Y. Q., Loughlin, D., Zheng, H. T., Zhao,
412 B., Liu, S. C., Smith, K. R., and Hao, J. M.: The quest for improved air quality may
413 push China to continue its CO₂ reduction beyond the Paris Commitment, Proc. Natl.
414 Acad. Sci. U. S. A., 117, 29535-29542, <https://doi.org/10.1073/pnas.2013297117>,
415 2021.

416 Xu, W., Song, W., Zhang, Y. Y., Liu, X. J., Zhang, L., Zhao, Y. H ., Liu, D. Y ., Tang, A.
417 H., Yang, D. W., Wang, D. D., Wen, Z., Pan, Y. P., Fowler, D., Collett, J. L.,
418 Erisman, J. W., Goulding, K., Li, Y., and Zhang, F. S.: Air quality improvement in
419 a megacity: implications from 2015 Beijing Parade Blue pollution control actions,
420 Atmos. Chem. Phys., 17, 31-46, <https://doi.org/10.5194/acp-17-31-2017>, 2017.